Acetone Reactions over the Surfaces of Polycrystalline UO2: A Kinetic and Spectroscopic Study

ARTICLE *in* LANGMUIR · MAY 2009

Impact Factor: 4.46 · DOI: 10.1021/la803933t · Source: PubMed

2 AUTHORS, INCLUDING:

Hicham Idriss
Saudi Basic Industries Corporation (SABIC)
235 PUBLICATIONS **4,837** CITATIONS

Langmuir
Article
pubs.acs.org/Langmuir

Acetone Reactions over the Surfaces of Polycrystalline UO_2: A Kinetic and Spectroscopic Study

Richard King[†] and Hicham Idriss*[,†,‡,§]

[†]*Department of Chemistry, The University of Auckland, Auckland, New Zealand,* [‡]*Department of Chemistry, Aberdeen University, Aberdeen, AB24 3 EU, U.K. and* [§]*Robert Gordon University, Aberdeen AB10 1FR, U.K.*

Received November 29, 2008. Revised Manuscript Received January 13, 2009

The reaction of acetone is studied on the surfaces of polycrystalline UO_2, prepared by hydrogen reduction of U_3O_8 at 770 K. The study is conducted by in situ Fourier transform infrared (FTIR) and temperature-programmed desorption (TPD). Acetone adsorption does not fit the simple Langmuir model, and adsorbate−adsorbate interactions are found to be significant. Acetone adsorbs molecularly on UO_2 as evidenced by the νC═O of the η^1(O) mode at 1686 cm^{-1}. Part of acetone is reduced to the isopropoxide species ($(CH_3)_2HC-O-U^{4+}$) upon heating (ν(CC), $\rho(CH_3)$ at 1167 cm^{-1} and ν(CO), $\rho(CH_3)$ at 980 cm^{-1}), and upon further heating, acetates (CH_3COO(a), (a) for adsorbed) are observed. Detailed TPD studies indicated that the main reaction of acetone on UO_2 is the deoxygenation to propene, driven by the oxophilic nature of UO_2. Other reactions were also observed to a lesser extent, and these included reductive coupling to 2,3-dimethylbutene and condensation to mesityl oxide. An attempt to extract kinetic parameters from TPD data was conducted. Three models were studied: variation of heating rate, leading edge analysis (Habenschaden−Kuppers method), and complete analysis. The complete analysis provided the most plausible results, in particular, at low coverage. With this method, at nearly zero coverage the activation energy, E_d, for desorption was found to be close to 140 kJ/mol with a prefactor of 10^{13} s^{-1}. E_d dropped sharply with increasing coverage, θ, to ca. 35 kJ/mol at $\theta = 0.15$ with a prefactor of 10^{11} s^{-1}. The activation energy for the desorption of acetone on UO_2(111) single crystals, at saturation coverage, was previously found to be equal to 65 kJ/mol using the leading edge analysis.

1. Introduction

With renewed interest in nuclear reactor technology for energy uses, our knowledge of the surface reactions of the oxides of actinides would become crucial, especially when related to environmental issues associated with storing depleted nuclear fuel. In that regard, our understanding of the surface reactions of the oxides of the actinides lags far behind that of the early transition metals. The ability of the outer 5f electrons in uranium to hybridize, allowing the element to exist in a wide range of oxidation states from +2 to +6, is a characteristic that potentially makes uranium compounds good model catalysts. Uranium oxides have been reported to catalyze several textbook-type reactions, including (i) dehydrogenation, (ii) oxidation, (iii) ammoxidation, (iv) oxidative coupling, and (v) esterification. (i) The dehydrogenation of primary alcohols such as ethanol has been reported over uranium oxides: UO_2, U_3O_8, and UO_3.[1−3] (ii) Total destruction of undesirable environmental volatile organic compounds (VOCs) by catalytic oxidation utilizing α-U_3O_8 was observed.[4−6] Nozaki and Ohki [7] have previously observed a high catalytic activity for the oxidation of carbon monoxide using α-U_3O_8 whereas UO_2^{2+} has been used as a catalyst for the photo-oxidation of hydrocarbons with molecular oxygen.[8] (iii) The ammoxidation of olefins, catalyzed by a uranium−antimony complex, USb_3O_{10}, has been reported by Grasselli and co-workers.[9−12] (iv) Oxidative coupling involves the formation of new carbon−carbon bonds and the oxidation of hydrocarbon molecules. Furan (C_4H_4O) has been produced over polycrystalline β-UO_3 from a variety of reactants including ethylene,[13] ethanol,[1] acetylene,[14] and acetaldehyde[15,16] in oxidative coupling reactions. By contrast, α-U_3O_8 does not catalyze this reaction; the reason is postulated to be due to the higher coordination number of uranium cations in U_3O_8 and is not due to the oxidation state because two-thirds of the uranium cations in U_3O_8 are in a +6 oxidation state. (v) Ai[17] described the esterification of formaldehyde catalyzed by various metal oxides including U_3O_8. This dimerization or Tischenko reaction requires the presence of both basic and acidic sites on the oxide surface; the products include methyl formate, formic acid, methanol, CO, and CO_2.

Ketones are in a special class among simple organic compounds. They typically undergo three types of reactions: (a) nucleophilic addition to the carbonyl carbon, (b) deoxygenation

*Corresponding author. E-mail: h.idriss@abdn.ac.uk.

(1) Madhavaram, H.; Idriss, H. *J. Catal.* **1999**, *184*, 553.
(2) Chong, S. V.; Griffiths, T. R.; Idriss, H. *Surf. Sci.* **2000**, *444*, 187.
(3) Chong, S. V.; Barteau, M. A.; Idriss, H. *Catal. Today* **2000**, *63*, 283.
(4) Taylor, S. H.; Heneghan, C. S.; Hutchings, G. J.; Hudson, I. D. *Catal. Today* **2000**, *59*, 249.
(5) Heneghan, C. S.; Hutchings, G. J.; O'Leary, S. R.; Taylor, S. H.; Boyd, V. J.; Hudson, I. D. *Catal. Today* **1999**, *54*, 3.
(6) Hutchings, G. J.; Heneghan, C. S.; Hudson, I. D.; Taylor, S. H. *Nature* **1996**, *384*, 341.
(7) Nozaki, F.; Ohki, K. *Bull. Chem. Soc. Jpn.* **1972**, *45*, 3473.
(8) Wang, W. D.; Bakac, A.; Espenson, J. H. *Inorg. Chem.* **1995**, *34*, 6034.
(9) Grasselli, R. K.; Burrington, J. D.; Suresh, D. D.; Friedrich, M. S.; Hazle, M. A. S. *J. Catal.* **1981**, *68*, 109.
(10) Grasselli, R. K.; Suresh, D. D. *J. Catal.* **1972**, *25*, 273.
(11) Grasselli, R. K.; Burrington, J. D. *Adv. Catal.* **1981**, *30*, 133.
(12) Grasselli, R. K.; Burrington, J. D.; Brazdil, J. F. *Faraday Discuss. Chem. Soc.* **1981**, *72*, 203.
(13) Madhavaram, H.; Idriss, H. *Stud. Surf. Sci. Catal.* **1997**, *110*, 265.
(14) Madhavaram, H.; Idriss, H. *J. Catal.* **2002**, *206*, 155.
(15) Madhavaram, H.; Idriss, H. *Catal. Today* **2000**, *63*, 309.
(16) Madhavaram, H.; Idriss, H. *J. Catal.* **2004**, *224*, 358.
(17) Ai, M. *J. Catal.* **1983**, *83*, 141.

reactions, and (c) α-hydrogen abstraction. (a) Potential nucleophiles encountered in surface chemistry are the hydride and hydroxide ions or water molecules, which react with acetone to give secondary alcohols or gem diols. (b) The deoxygenation of acetone results in propene, and this reaction has been observed on both oxidized and reduced TiO_2(001) single-crystal surfaces.[18] (c) α-H abstraction results in the formation of the acetone enolate, a reaction that has been widely observed on metal oxides including MgO,[19,20] NiO,[20] SnO_2,[21] γ-Al_2O_3,[22] and α-Fe_2O_3.[23] Acetone enolate is formed by the acid- or base-catalyzed abstraction of hydrogen from a methyl group or from the OH group of the enol tautomer. Typically, this involves an acetone molecule bound through oxygen to a Lewis acid site, and the α-H is abstracted by a surface OH^- or O^{2-} in close proximity. The enolate is an intermediate in the aldol condensation reaction. Aldol condensation of acetone has been observed on TiO_2 powder,[24,25] on UO_2(111) single crystals[26] and on acidic catalysts.[27] This reaction involves the nucleophilic addition of a second acetone molecule to an enolate with the subsequent loss of water to form mesityl oxide.

A relatively less known route for acetone in catalysis and surface chemistry is that leading to larger compounds by reductive coupling. Two classes of reductive coupling reaction have been observed in organic heterogeneous systems involving ketone substrates: either coupling to form pinacols or the formation of olefins. The reaction to form pinacols has a long history and has traditionally utilized the alkali metals as well as Mg/MgI_2 mixtures[28] or Al/Hg amalgams[29] as catalysts. However, a wide range of transition metals and lanthanides are also active in this reaction.[30] It has been found that aromatic ketones more readily undergo this type of reaction than do aliphatic ketones because the aromatics are more easily reduced. The formation of olefins is a more recent discovery,[30] and the range of active catalysts is more limited. Low-valent titanium catalysts ($TiCl_3$/Zn−Cu,[31] $TiCl_3$/$LiAlH_4$,[32] reduced UO_2(111),[16,26] and TiO_2(001) single crystals [18,33−35]) have been found to be the most active and are capable of acting on both aromatic and aliphatic substrates. Both classes of reductive coupling reactions are thought to share a common path: they proceed first with the reduction of the carbonyl to a radical anion (ketyl), followed by coupling to form the new carbon−carbon bond; the pinacol dianion is then either protonated in the final step to form the diol or deoxygenated to yield the alkene. The deoxygenation of the resulting metallopinacol is likely to be the rate-determining step of the reaction sequence according to McMurray.[36] An alternative mechanism for the reductive coupling of ketones has been proposed from the study of tungsten complexes.[37−40] This route involves the deoxygenation of the ketone to form a metal carbene, followed by the reaction of this intermediate with a second ketone molecule to form an alkene product.

Acetone is known to undergo reductive coupling to form 2,3-dimethylbutene in good yield in organometallic chemistry using a uranium catalyst, UCl_4−Na(Hg) or UCl_4−Li(Hg).[41] These studies provide evidence that the reaction proceeds via a pinacol intermediate, and Pierce and Barteau[18] have proposed that it is McMurray's mechanism that is active in the gas−solid heterogeneous catalysis of ketones involving TiO_2 surfaces.

The main reactions of acetone on the surfaces of UO_2 are expected to be the following:

$$2CH_3COCH_3 \rightarrow H_2O + (CH_3)_2C{=}CHCOCH_3 \text{ (mesityl oxide)} \quad (1)$$

$$2CH_3COCH_3 \rightarrow 2[O] + (CH_3)_2C{=}C(CH_3)_2 \text{ (dimethylbutene)} \quad (2)$$

$$CH_3COCH_3 \rightarrow [O] + CH_2{=}CHCH_3 \text{ (propene)} \quad (3)$$

$$CH_3COCH_3 + 2[H] \rightarrow CH_3CH(OH)CH_3 \text{ (isopropanol)} \quad (4)$$

In this work, the reaction of acetone over polycrystalline UO_2 is investigated by infrared spectroscopy (IR) and temperature-programmed desorption (TPD). The IR experiments were performed to determine the nature of surface adsorbates, and the TPD experiments provided details of product distribution and kinetic parameters, the activation energy, and the pre-exponential factor.

2. Experimental Section

Powder samples of the staring material, commercial-grade U_3O_8 (BDH), and the hydrogen-reduced product were analyzed by XRD. The XRD system comprised a Philips PW 1130 high-voltage generator (40 kV, 20 mA) utilizing a copper anode X-ray tube. A Philips PW 1050/25 goniometer, fitted with a PW 1752 curved graphite crystal monochromator and a PW 1965 proportional detector, was used. The incident X-ray wavelength was 1.54056 Å (Cu K1α). The crystal structures were identified by matching the peak positions and intensity with known standards held by the Joint Committee on Powder Diffraction Standards (JCPDS).

For the transmission IR spectroscopy system, the uranium oxide powder sample was made into a compressed disk and

(18) Pierce, K. G.; Barteau, M. A. *J. Org. Chem.* **1995**, *60*, 2405.
(19) Sanz, J. F.; Oviedo, J.; Marquez, A.; Odriozola, J. A.; Montes, M. *Angew. Chem., Int. Ed.* **1999**, *38*, 506.
(20) Miyata, H.; Toda, Y.; Kubokawa, Y. *J. Catal.* **1974**, *32*, 155.
(21) Thornton, E. W.; Harrison, P. G. *J. Chem. Soc., Faraday Trans. 1* **1975**, *71*, 2468.
(22) Hanson, B. E.; Wieserman, L. F.; Wagner, G. W.; Kaufman, R. A. *Langmuir* **1987**, *3*, 549.
(23) Busca, G.; Lorenzelli, V. *J. Catal.* **1980**, *66*, 155.
(24) El-Maazawi, M.; Finken, A. N.; Nair, A. B.; Grassian, V. H. *J. Catal.* **2000**, *191*, 138.
(25) Zaki, M. I.; Hasan, M. A.; Pasupulety, L. *Langmuir* **2001**, *17*, 768.
(26) King, R. I.; Senanayake, S. D.; Chong, S. V.; Idriss, H. *Surf. Sci.* **2007**, *601*, 5690.
(27) Panov, A.; Fripiat, J. J. *Langmuir* **1998**, *14*, 3788.
(28) Gomberg, M.; Bachman, W. E. *J. Am. Chem. Soc.* **1927**, *49*, 236.
(29) Schreibmann, A. *Tetrahedron Lett.* **1970**, 4271.
(30) Kahn, B. E.; Rieke, R. D. *Chem. Rev.* **1988**, *88*, 733.
(31) McMurry, J. E.; Fleming, M. P.; Kees, K. L.; Krepski, L. R. *J. Org. Chem.* **1978**, *43*, 3255.
(32) McMurry, J. E.; Fleming, M. P. *J. Am. Chem. Soc.* **1974**, *96*, 4708.
(33) Idriss, H.; Barteau, M. A. *Stud. Surf. Sci. Catal.* **1993**, *78*, 463.
(34) Idriss, H.; Pierce, K. G.; Barteau, M. A. *J. Am. Chem. Soc.* **1994**, *116*, 3063.
(35) Idriss, H.; Barteau, M. A. *Langmuir* **1994**, *10*, 3639.
(36) McMurry, J. E. *Chem. Rev.* **1989**, *89*, 1513.
(37) Chisholm, M. H.; Folting, K.; Klang, J. A. *Organometallics* **1990**, *9*, 602.
(38) Chisholm, M. H.; Folting, K.; Klang, J. A. *Organometallics* **1990**, *9*, 607.
(39) Bryan, J. C.; Mayer, J. M. *J. Am. Chem. Soc.* **1990**, *112*, 2298.
(40) Fujiwara, Y.; Ishikawa, R.; Akiyama, F.; Teranishi, S. *J. Org. Chem.* **1978**, *43*, 2477.
(41) Maury, O.; Villiers, C.; Ephritikhine, M. *Angew. Chem., Int. Ed. Engl.* **1996**, *35*, 1129.

mounted within a purpose-built IR cell (University of Auckland), constructed from stainless steel and equipped with water-cooled crystal windows composed of either calcium fluoride or zinc selenide. The cell could be electrically heated to 800 K or cooled with liquid nitrogen. Temperature measurements were made using a K-type thermocouple placed in close proximity to the sample. During experiments, the cell was evacuated to a base pressure of $\sim 2 \times 10^{-5}$ Torr. The vacuum was maintained by two roughing pumps and an oil diffusion pump, and pressure measurements were made with one Penning and one Pirani gauge. Fourier transform infrared (FTIR) spectroscopy was performed using a Biorad-Digilab FTS-60 spectrometer at a resolution of 4 cm^{-1} and 100 scans per spectrum. Acetone (Panreac, analytical grade), degassed by several freeze−pump−thaw cycles, was introduced into the system from a glass bulb and was allowed to equilibrate with the powder sample at known pressure; the cell was then pumped to base pressure for the recording of spectra.

For the temperature-programmed desorption (TPD) system, a glass reaction chamber was used, into which a measured amount ($\sim$1 g) of the powdered uranium dioxide was placed. The reactor was connected to the mass spectrometer via a leak valve, and the whole system was evacuated to $\sim 1 \times 10^{-7}$ Torr by a diffusion pump (Edwards E02). Acetone (Panreac, analytical grade), degassed by serial freeze−pump−thaw cycles, was introduced into the system via syringe and allowed to equilibrate at room temperature for 5 min; the chamber was then pumped for 10 min to remove any nonadsorbed molecules. A furnace was connected to a temperature controller providing a linear temperature ramp to heat the sample; desorbing species were identified by quadrupole mass spectrometry. Blank runs, with no uranium dioxide and following reduction by hydrogen but without the injection of acetone, were also completed. The uranium dioxide substrate was rejuvenated between experiments by reduction under hydrogen flow at 770 K for 12 h.

A high pumping speed was maintained relative to the reactor volume, and low heating rates were used (0.1 to 0.4 K s^{-1}), with the intention being to keep the pressure changes within the hamber low, thus ensuring that the desorption rate was directly proportional to the pressure increase or the count rate recorded by the mass spectrometer. The pumping speed of the diffusion pump with a liquid-nitrogen trap is 150 L/s. We assume that one monolayer of desorption from a 10 m^2/g catalyst (the surface area of the UO_2 powder) equal to 0.3×10^{19} molecules/m^2 gives 0.3×10^{20} molecules. This is equal to 0.0012 L (to be compared to 150 L/s). The mass spectrometer signal recorded against time was combined with the temperature ramp to produce a spectrum of the desorption rate against temperature.

The area under each peak is proportional to the quantity of the species desorbed from the surface (eq 5)

$$\frac{dN}{dt} = P \qquad N = \int P\, dt \tag{5}$$

where N is the number of molecules desorbing and P is the partial pressure increase. The area under each peak was calculated by integration using the trapezoid rule.

The relative yield for each species (Y_i) was obtained as a fraction of the sum of the total products,

$$Y_i = \frac{A_i CF_i}{\sum_j^n A_j CF_j} \tag{6}$$

where A_i is the area under the peak and CF_i is the correction factor for species i.[42] The correction factor relative to carbon monoxide was calculated according to the method outlined by Ko et al.[43]

3. Results and Discussion

A standardized method for the preparation of uranium dioxide was used in both the temperature-programmed desorption studies and the infrared experiments. UO_2 was prepared by the reduction of U_3O_8 under a flow of hydrogen at 770 K for 12 h. Confirmation that the reduction had taken place was obtained by X-ray diffraction (XRD) (Figure 1). The peak positions and relative intensities are given in the inset of the Figure and show good agreement with reference values published by JCPDS.

3.A. Infrared Spectroscopy. Before presenting the IR data, it is worth indicating the two main modes of adsorption of carbonyls in general and for acetone in this case. Acetone has been observed to adopt two binding modes on metals and metal oxide surfaces. The first bonding configurations of acetone to be considered is through the relatively electron-rich carbonyl oxygen that acts as a Lewis base; it donates a lone pair of electrons to form a σ bond with an acidic site. Binding through the lone pair on the oxygen, referred to as η^1(O) (Scheme 1) results in a reduction in the electron density within the carbon−oxygen bond, as indicated by the red shift in its frequency, from 1730 cm^{-1} observed in the gas phase to a value typically between 1670 and 1690 cm^{-1}. The other bonds in the carbon skeleton are not significantly affected in this adsorption mode, so their vibrational frequencies are observed at values close to those seen in the gas phase. The η^1(O) adsorption mode has been observed experimentally on many metals.[24,25,44−47]

The second bonding mode, designated η^2(O, C) (Scheme 1), involves both the carbon and oxygen atoms of the carbonyl group. Donation of the π electrons from the carbonyl bond to the metal d orbital and associated back-donation of electrons from the metal d orbital into the π^* orbital occur. Bonding is thus side-on as opposed to end-on, as seen in the case of η^1(O), and the corresponding effect on the strength of the carbonyl bond is much greater as indicated by a larger shift in its vibrational frequency. In this configuration, the carbonyl bond is typically observed as low as 1400 cm^{-1}. The other bonds within the carbon skeleton are also more heavily influenced in this configuration and display a shift in frequency not observed in the η^1(O) mode. The η^2(C, O) mode has been observed experimentally on Ru (001),[48] Pd(111),[49] and Pt(111)[50] metals.

The spectrum obtained on exposure of a hydrogen-reduced uranium dioxide surface to successive doses of gas phase acetone at 220 K is shown in Figure 2. The vibrational frequencies (cm^{-1}) of the observed peaks are given in Table 1, along with possible assignments. In this spectrum, the adsorption peaks assigned to the carbonyl (C═O) group are red shifted (with respect to the gas phase) to 1686 cm^{-1}, and the peaks assigned to the other bonds within the carbon skeleton

(42) Yee, A.; Morrison, S. J.; Idriss, H. *J. Catal.* **1999**, *186*, 279.

(43) Ko, E. I.; Benziger, J. B.; Madix, R. J. *J. Catal.* **1980**, *62*, 264.
(44) Henderson, M. A. *J. Phys. Chem. B* **2004**, *108*, 18932.
(45) Mattsson, A.; Leideborg, M.; Larsson, K.; Westin, G.; Sterlund, L. *J. Phys. Chem. B* **2006**, *110*, 1210.
(46) Panov, A.; Fripiat, J. J. *J. Catal.* **1998**, *178*, 188.
(47) Griffiths, D. M.; Rochester, C. H. *J. Chem. Soc., Faraday Trans. 1* **1978**, *74*, 403.
(48) Anton, A. B.; Avery, N. R.; Toby, B. H.; Weinberg, W. H. *J. Am. Chem. Soc.* **1986**, *108*, 684.
(49) Davis, J. L.; Barteau, M. A. *Surf. Sci.* **1989**, *208*, 383.
(50) Avery, N. R. *Surf. Sci.* **1983**, *125*, 771.

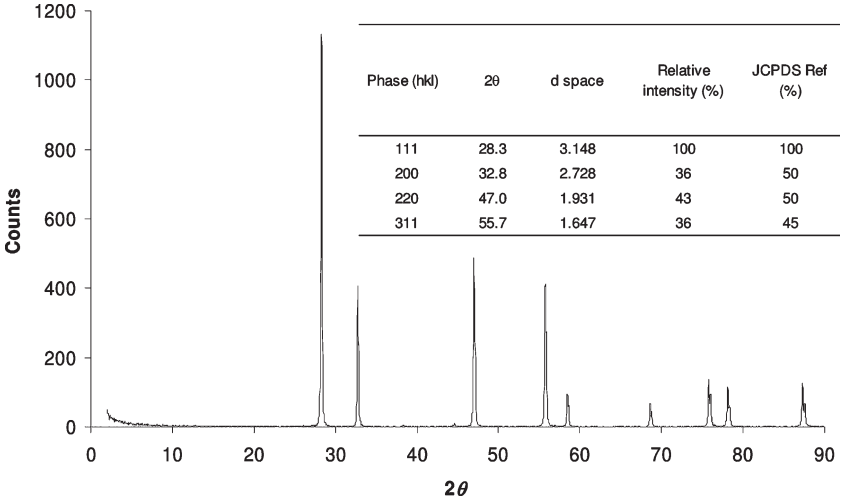

Figure 1. XRD spectrum of polycrystalline UO_2 prepared by the hydrogen reduction of α-U_3O_8.

Scheme 1. Two binding modes of acetone: (a) η^1(O) and (b) η^2(O, C).

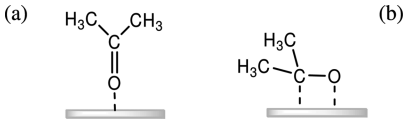

of adsorbed acetone are similar to those in the gas or condensed phase. Also listed in Table 1 are the assignments of acetone adsorbed in the η^1(O) mode to titanium[44,45] aluminum, cerium, and zirconium oxides[46] and to p(2 × 2) O−ruthenium(001) [48] and p(2 × 2) O−rhodium(111)[51] metal surfaces. There is close agreement between the observed vibrational frequencies in this work and those listed, suggesting that acetone is predominantly adsorbed molecularly and in the η^1(O) mode. At higher acetone exposures, a shoulder centered at 1702 cm^{-1} developed on the 1686 cm^{-1} (C═O) peak. This was associated with a shift in the peak at 1248 to 1235 cm^{-1} and the development of a shoulder at 991 cm^{-1}. On heating, these changes were reversed (Figure 3a), with the loss of the 1702 cm^{-1} peak occurring before the loss of the 1686 cm^{-1} peak, as shown by the reduction in relative intensities plotted in Figure 4. The vibration at 1702 cm^{-1} is close to the frequency of C═O in condensed-phase acetone, and the shift in the 1248 cm^{-1} peak is toward the 1221 cm^{-1} frequency observed in the condensed phase; a vibration at 993 cm^{-1} is also seen in the condensed phase. This suggests that at higher exposures a condensed multilayer may be forming, a phenomenon also reported on the TiO_2(110)[44] and Pt(111)[50] surfaces. The temperature-programmed desorption data in this study also shows a low-temperature nonsaturating peak suggestive of the formation of a condensed multilayer.

Peaks in addition to those assigned to adsorbed acetone were observed at 1190, 1130, 733, and 715 cm^{-1}, and their origins will be discussed next.

The adsorption of acetone onto 0.25-O Ag(110)[52] and Ag (111)[53] single-crystal surfaces gave peaks at 1190 cm^{-1} assigned by the authors to the ν_a(OCO) vibration of a $(CH_3)_2COO_{(a)}$ species. The symmetric stretching vibration, ν_s(OCO), occurs as a combination peak with the methyl rocking vibration, $\rho(CH_3)$, and the carbon−carbon stretch,

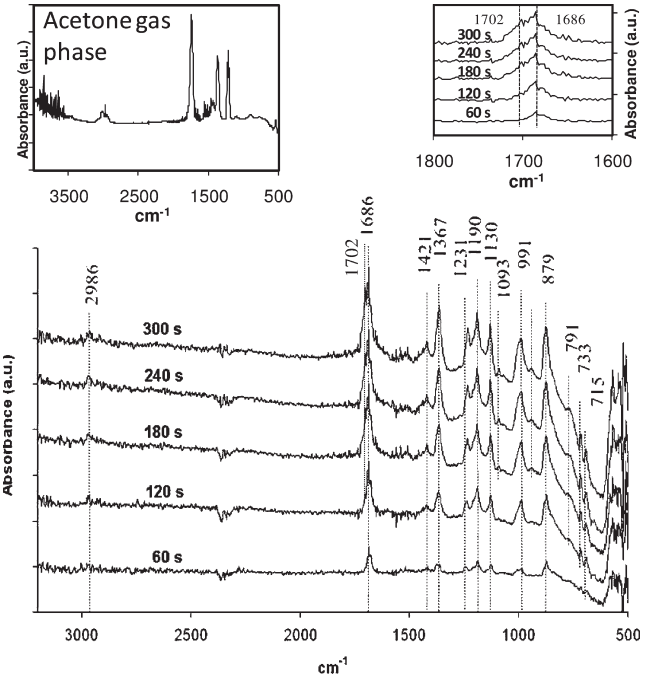

Figure 2. IR spectra of acetone adsorbed on polycrystalline UO_2 at 220 K with increasing exposure. Times indicate the cumulative exposure time to acetone at 7.0 × 10^{-2} Torr. (Right-hand inset) νC═O region indicating the appearance of the 1702 cm^{-1} peak after the 1686 cm^{-1} peak.

ν(CCC), at 980 cm^{-1}. In this study, the broad peak observed at 995 cm^{-1} may have obscured any peak at 980 cm^{-1}. A bending vibration of the O−C−O bond, δ(OCO), was observed at 580 cm^{-1} on the oxygen-activated Ag(110) surface, and a poorly resolved peak appears at 570−580 cm^{-1} in this work. This is, however, at the limit of transmission of the zinc selenide windows used in the experiment. It is worth noting that this species is fundamentally different from that of acetates $CH_3COO_{(a)}$, although the former might be seen as a precursor to the later. The $(CH_3)_2COO_{(a)}$ species contains two single carbon−oxygen bonds, whereas the acetate contains a delocalized double bond in addition.

TPD data revealed propene as a major product (see next section). It seems reasonable to postulate that the intermediate in this deoxygenation reaction is an isopropoxide. To test this hypothesis and investigate if this intermediate could

(51) Houtman, C.; Barteau, M. A. *J. Phys. Chem.* **1991**, *95*, 3755.
(52) Ayre, C. R.; Madix, R. J. *J. Am. Chem. Soc.* **1995**, *117*, 2301.
(53) Sim, W. S.; King, D. A. *J. Phys. Chem.* **1996**, *100*, 14794.

Table 1. Observed Frequencies and Assignments for Gas-Phase and Condensed-Phase Acetone and Acetone Adsorbed to Various Metals and Oxides[a]

	acetone		TiO_2							
	gas phase	cond phase	ref [2]	ref [1]	Al_2O_3 [3]	ZrO_2 [3]	CeO_2 [3]	p(2 × 2)O−Ru(001) [5]	p(2 × 2)O-Rh(111) [8]	UO_2 (this work)
ν(CO)	1731 vs	1710 s	1702	1690	1702/1675 s/m	1703	1695/1672	1690	1665	1686
ν_a(CCC)	1215 vs	1221 m	1240	1210	1236 m	1229			1240	1231
ν_s(CCC)	777 w	787 vs						825/780		791
δ(CO)	530 s	531 m								
δ(CCC)	484 w	493 w								
π(CO)	385 w	393 w								
$\nu(CH_3)$	2972 s	2967 s	2973			2962		2950	2980	2986
	2937 s	2922 vs	2931	2945		2931				
$\delta(CH_3)$	1435 s	1430 s	1422	1400	1451/1422 w	1467/1422 w		1440	1410	1421
	1363 vs	1356 w	1366	1350	1370 m	1367		1395	1350	1367
	1090 m	1092 m		1055				900	930	1093
		995								
$\omega(CH_3)$	891 m	1066 m								879
		902 w								

[a] w = weak, m = medium, s = strong, and vs = very strong.

account for the unassigned peaks, isopropanol was adsorbed onto the hydrogen-reduced surface of UO_2 (Figure 5). Previous studies of isopropanol adsorption onto oxides[54−56] have shown that dissociative adsorption to form isopropoxides occurs concurrently with molecular adsorption through the oxygen. The adsorbed isopropoxide may account for the peak at 1130 cm^{-1} that is characteristic of the combined ν(CC), ν(CO), and $\rho(CH_3)$ frequencies (Table 2). The other peaks for adsorbed isopropoxide are close to those of acetone, with both species having similar structures, and are likely to be superimposed on the corresponding peaks observed in this study.

In the spectra showing the effect of temperature on the adsorbed species (Figure 6), there appears to be a relationship between the peaks at 956 and 1167 cm^{-1} and between the peaks at 995 and 1132 cm^{-1}. This relationship appears to be stronger between the latter two peaks; their relative intensities plotted in the inset track each other very closely. These two sets of peaks are likely to represent two different species adsorbed on the oxide surface.

The peaks at 733 and 715 cm^{-1} in the acetone adsorption spectra are at present unassigned.

Following the adsorption of acetone onto the sample, the stability of the adsorbed species was investigated. IR spectra were recorded after heating the complex in incremental steps to a temperature of 800 K. The sample was subsequently cooled to 100 K to record the spectra shown in Figure 3a,b. Loss of adsorbed acetone was seen by approximately 500 K. This finding was in general agreement with the TPD experiments (see next section). The 1130 cm^{-1} peak assigned to the adsorbed isopropoxide was also lost at a similar temperature. Associated with the loss of the peaks assigned to the adsorbed acetone and isopropoxide, a broad peak at 783 cm^{-1} with a shoulder at 750 cm^{-1} develops. This may represent the oxidation of the substrate to U_3O_8. Allen et al.[57] have assigned a combination band and a fundamental stretching vibration in the −O−U−O−U−O− chain to 780 and 745 cm^{-1}, respectively.

An alternative assignment for this peak would be the formation of acetone enolate ($CH_2{=}C(CH_3)O_{(a)}$) in which $\gamma(=CH_2)$ is at 790 cm^{-1};[52] however, this is an unlikely assignment in this case because the accompanying, relatively strong peaks at 1040, 1300, 1340, 1420, and 1545 cm^{-1},[44,46,52,53,58,59] indicative of this structure, do not appear in the spectrum.

At higher temperatures above 500 K, absorption peaks at 1440 and 1550 cm^{-1} were observed (Figure 3b) with an associated small peak at 1325 cm^{-1}. (Note that in Figure 3b the experiment was repeated using CaF_2 windows). Prominent peaks in the ν(CH) region, centered at 2965, 2930, and 2859 cm^{-1}, were also seen. These peaks can be assigned to an acetate species and have been observed at high temperatures in other work on oxide surfaces.[44] The peak of gas-phase carbon dioxide, centered at 2349 cm^{-1}, was noted to increase in successive spectra, indicating its formation with rising temperature. This is consistent with the evolution of carbon dioxide at high temperature (above 600 K) noted in the TPD spectra. The high-temperature decomposition of acetates is a likely source of this carbon dioxide. The observed species in associated reaction steps are summarized in Scheme 2.

3.B. Temperature-Programmed Desorption. TPD experiments were performed to identify the products of the interaction of acetone with the oxide surface and to calculate the kinetic properties for the desorption reaction. The reaction products and the relative yields will be discussed first; calculation of the activation energy will be examined in the second section.

3.B.1. Fragmentation Patterns. To interpret the mass spectrometry data, fragmentation patterns for acetone and the likely reaction products were required. The principal reactions observed involving ketones over metal and metal oxides are given by eqs 1−4. The products of these reactions using acetone as the reagent are mesityl oxide, 2,3-dimethylbutene, propene, and isopropanol. The fragmentation patterns for acetone and these reaction products are given in Table 3.

The fragmentation patterns for acetone, mesityl oxide, and isopropanol were obtained experimentally after the injection of pure samples of each product. The patterns for 2,3-dimethylbutene and propene were obtained from

(54) Rossi, P. F.; Busca, G.; Lorenzelli, V.; Saur, O.; Lavalley, J. C. *Langmuir* **1987**, *3*, 52.
(55) Zaki, M. I.; Sheppard, N. *J. Catal.* **1983**, *80*, 114.
(56) Hussein, G. A. M.; Sheppard, N.; Zaki, M. I.; Fahim, R. B. *J. Chem. Soc., Faraday Trans. 1* **1989**, *85*, 1723.
(57) Allen, G. C.; Crofts, J. A.; Griffiths, A. J. *J. Nucl. Mater.* **1976**, *62*, 273.
(58) Martin, C.; Martin, I.; Rives, V. *J. Catal.* **1994**, *145*, 239.
(59) Miyata, H.; Toda, Y.; Kubokawa, Y. *J. Catal.* **1974**, *32*, 155.

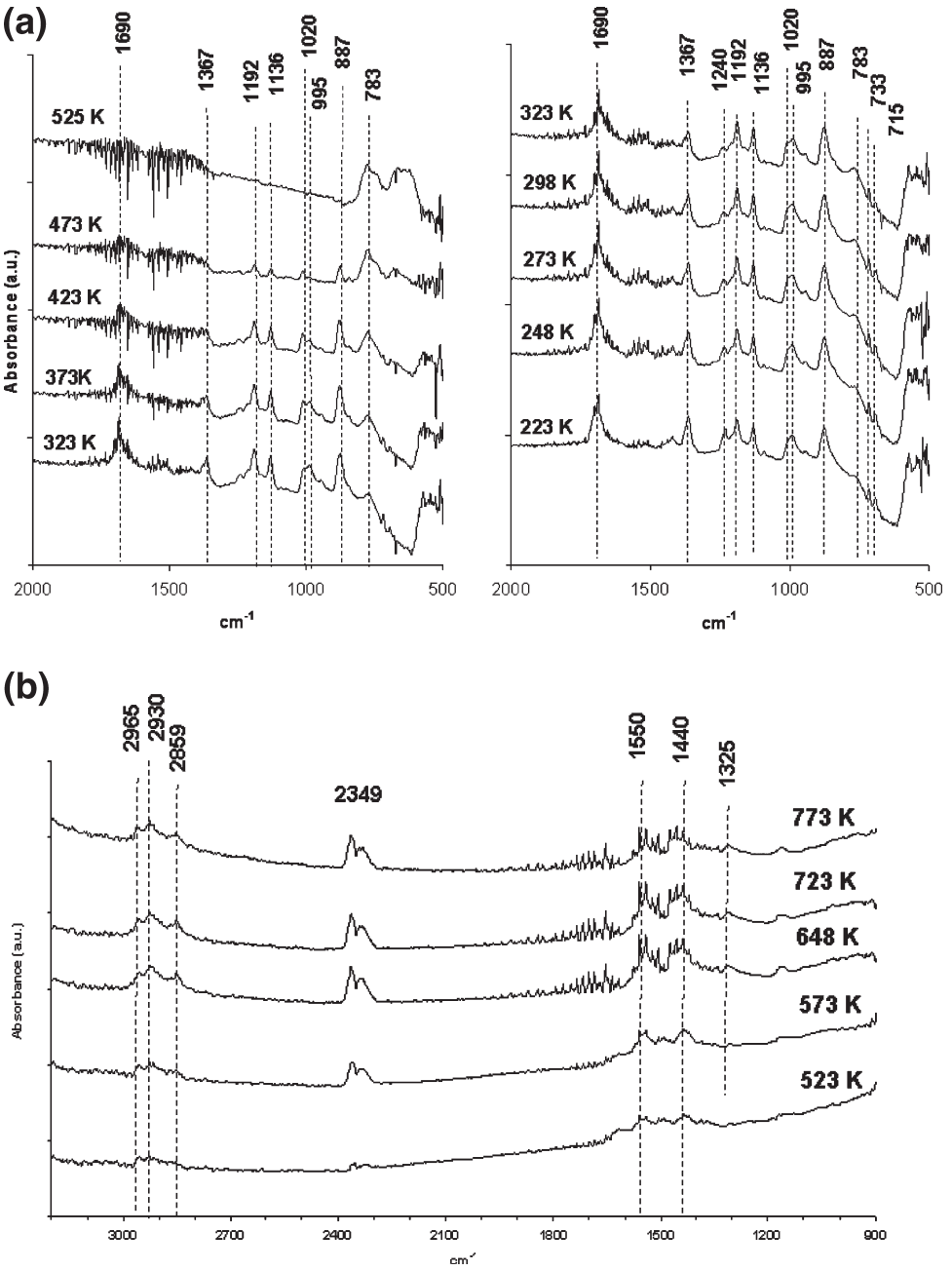

Figure 3. (a) IR spectra of acetone adsorbed on polycrystalline UO_2 at 220 K and the effect of incremental heating to the indicated temperatures (220−525 K). (b) IR spectrum of acetone adsorbed on polycrystalline UO_2 at 220 K and the effect of heating to incremental temperatures (523−773 K). Spectra were recorded using a cell fitted with CaF_2 windows.

reference tables. Comparing the fragmentation patterns of those samples that were obtained from this instrument with reference data shows that there was a bias toward the smaller-mass fragments from the experimental cracking patterns. This will have introduced a systematic error into the calculation of the relative abundance of the various products; it is likely that the reported abundance for 2,3-dimethylbutene, in particular, was underestimated because the identification of this species is dependent on the large mass fragment, m/z 69.

3.B.2. Product Distribution. The product distribution was obtained at saturation coverage after the injection of 20 μL of liquid acetone (about 10^{20} acetone molecules; 1 g of UO_2 has a BET surface area of about 10 m^2 or about 10^{20} surface U and O atoms) and at a heating rate of 0.25 K s^{-1}. The TPD trace recorded for the major mass fragments, m/z 15, 39, 43, and 58, shown in Figure 7 has three peaks—two unresolved peaks at 340 and 370 K and a broad peak centered at 520 K. A fourth peak at 750 K was also observed but was not included in the analysis because the trace had not returned to the baseline upon completion of recording. The inset in Figure 7 presents acetone desorption from UO_2(111) single crystals from our previous work.[26] A similar pattern is seen with three peaks desorbing at 380, 415, and 470−480 K. Although desorption temperatures deviate by 30 to 40 K, the shape of desorption bears good resemblance to the polycrystalline TPD. It is worth mentioning that the most stable phase in the fluorite structure is the [111] oriented as seen in Figure 1. The presence of multiple peaks suggests that multiple binding sites for the acetone molecule may be present on the surface. The major fragments were recorded in all spectra and were used to standardize the traces between

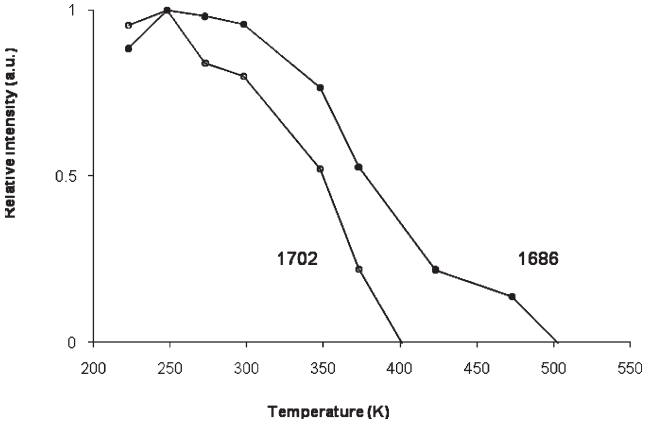

Figure 4. Relative intensities of adsorption peaks at 1701 and 1686 cm^{-1} attributed to the ν(C═O) mode, with the temperature for acetone adsorbed on polycrystalline UO_2 at 220 K.

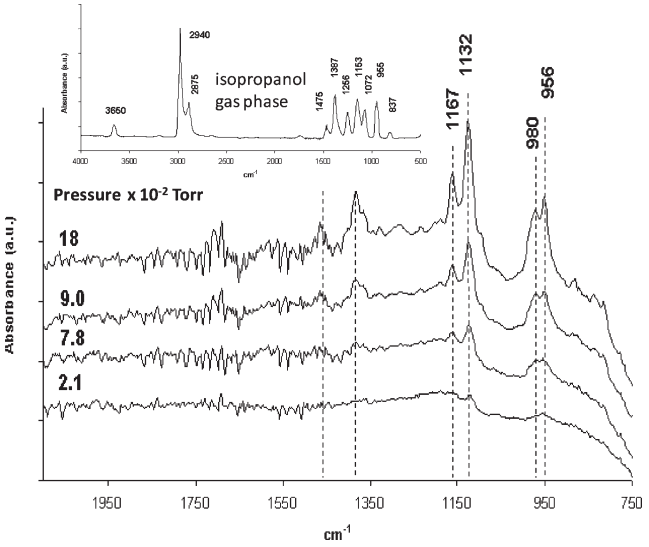

Figure 5. IR spectrum of isopropanol adsorbed on polycrystalline UO_2 at 220 K.

runs in order to calculate the relative abundance of the individual products.

From the fragmentation patterns given in Table 3, unique mass fragments for the various products were identified for mesityl oxide (m/z 83), 2,3-dimethylbutene (m/z 69), propene (m/z 42), and isopropanol (m/z 45). Figure 8 shows the TPD trace recorded for each of these fragments, indicating that all of the principal reaction classes—aldol condensation, reductive coupling, deoxygenation, and reduction—reported on other oxide surfaces appear to be active on UO_2. Unreacted acetone was identified from m/z 58. In addition, decomposition products carbon dioxide, water, and hydrogen were identified by mass fragments 44, 18, and 2, respectively (not shown).

In determining the relative abundances, the unique mass fragments were used first, and the ratios obtained were used to subtract the appropriate ratio for the smaller mass fragments until all had been apportioned. The product distribution given in Table 4 shows unreacted acetone constituting the major species (45%); of the reactions that took place, the deoxygenation reaction to propene was the largest at 80.7%, suggesting that it has the lowest energy and the most facile pathway. This is similar to a previous qualitative study on a

Table 2. IR Assigments for Gas-Phase and Adsorbed Isopropanol

assignments	gas (liquid) phase[14]	TiO_2 isopropoxide[11]	ZrO_2[13]	UO_2 (this work)
ν(OH)	3650		3550	
$\nu_a(CH_3)$	(2976)	2974	2970	2970
$\nu_s(CH_3)$	2940	2936		2940
ν(CH)	2875	2872	2865	
$2\delta_a(CH_3)$		2895	2930	
$\delta_a(CH_3)$	1475, 1460	1466, 1454	1465	1472
$\delta_s(CH_3)$	1387, 1367	1382, 1369	1380	1391
γ(CH)	1340	1342	1340	
δ(CH), δ(OH)	1266, 1256, 1246			
ν(CC), $\rho(CH_3)$	1153	1165		1167
	1130	1148	1130	1132
ν(CO), $\rho(CH_3)$	1072		1170	980
	955	1125	1030	956

similar material.[60] This may reflect the oxophilic nature of UO_2. The next major product was from the aldol condensation reaction yielding mesityl oxide (11%), followed by reduction/hydrogenation to isopropanol (3.7%) and the reductive coupling reaction to form 2,3-dimethylbutene (3.7%). A small amount of carbon dioxide (1%) was detected at high temperature (above 600 K). As indicated previously, the use of reference values for the fragmentation patterns of propene and especially 2,3-dimethylbutene may have resulted in an underestimation of the relative abundance of these products.

The exact stoichiometry of the polycrystalline surface studied in this work is not known; it is likely, from the method of preparation, to lie in the region of UO_{2+x} (x = 0.02−0.10); more aggressive reduction than that employed in this work is required to attain UO_2 and UO_{2-x}.[61−64] The results indicate that UO_{2+x} has a similar reactivity toward acetone as that observed for mildly reduced TiO_2.

3.B.3. Coverage Dependence. The coverage dependence of the TPD profile for acetone was determined using m/z 15, the major fragment, and m/z 58, the unique fragment for acetone. The plot of the change in pressure (desorption rate) against temperature for m/z 15 and 58 masses showed two peaks (Figure 9). The first peak at 340 K appeared only at high coverage (after the injection of 15 and 30 μL of acetone) and did not move significantly with increasing coverage. The peak maximum of the second peak moved to lower temperature with increasing coverage. This is suggestive of a reaction that is second order with constant activation energy or first order in which there are repulsive interactions; the activation energy decreases with increasing coverage due to the weakening of the surface−adsorbate interaction as the adsorbate−adsorbate interaction becomes stronger as a result of crowding.

The reaction of acetone with the surface to give a molecularly bound η^1(O) species (IR data) is likely to be zero or first order; such reactions typically give asymmetric peaks where the peak maximum and hence the activation energy is independent of coverage. to understand and model the adsorption process, it is common to construct an adsorption isotherm, a plot of the amount of gas adsorbed as a function of the gas pressure, where * represents an adsorption site as

(60) Madhavaram, H.; Idriss, H. *J. Vac. Sci. Technol., A* **1997**, *15*, 1685.
(61) Allen, G. C.; Crofts, J. A.; Curtis, M. T.; Tucker, P. M.; Chadwick, D.; Hampson, P. J. *J. Chem. Soc., Dalton Trans.* **1974**, 1296.
(62) Abrefah, J.; Dooley, D. F.; Olander, D. R. *J. Phys. Chem.* **1990**, *94*, 1937.
(63) Anderson, J. S.; Sawyer, J. O. *Proc. Chem. Soc. London* **1960**, 145.
(64) Saito, Y. *J. Nucl. Mater.* **1974**, *51*, 112.

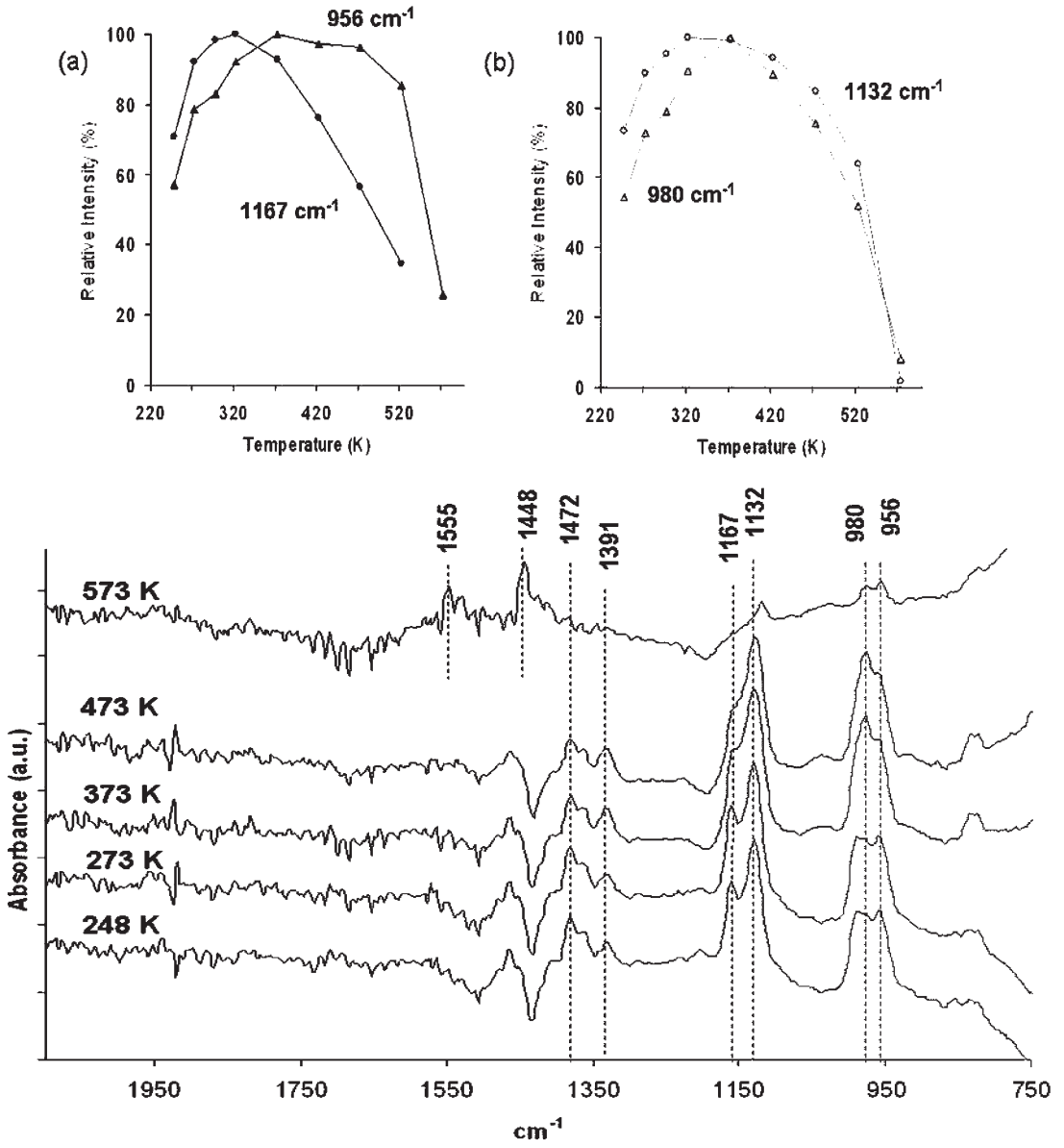

Figure 6. IR spectrum of isopropanol adsorbed on polycrystalline UO_2 at 220 K; effect of heating to incremental temperatures (220−573 K). (Inset) Plots showing the relationship between the relative intensity of (a) 956 and 1167 cm^{-1} peaks and (b) the 995 and 1132 cm^{-1} peaks with temperature.

shown in Scheme 3, where θ = coverage, $K_{ads} = k_1/k_2$ (the rate constants for evaporation and condensation on the surface), and P = pressure.

The resulting plot (Figure 10A) is nonlinear, suggesting that the Langmuir isotherm is not an appropriate model to use in this instance. It is assumed in the Langmuir equation that the adsorbing molecules have no lateral interactions. A simple modification of the Langmuir isotherm to account for lateral interactions is given by Adamson and Gast.[65] They state that the probability of a binding site being occupied is N/S, where N is the number of molecules present and S is the total number of surface sites available. If each site has z neighbors, then the probability of a neighboring site being occupied is zN/S. Therefore, the fraction of adsorbed molecules involved is $z\theta/2$, with the factor of $^1/_2$ accounting for double counting. If the lateral interaction energy is ω, then the added energy of adsorption becomes $z\omega\theta/2$ and the added differential energy of adsorption is $z\omega\theta$. The modified Langmuir equation becomes

$$\theta = \frac{K'[P]}{1 + K'[P]} \tag{7}$$

$$K' = k_0 \exp\left(\frac{Q + z\omega\theta}{RT}\right) = K_{ad} \exp \frac{z\omega\theta}{RT} \tag{8}$$

where Q is the activation energy and the other symbols are as previously defined. If this isotherm is used, then by plotting the volume of acetone added (proportional to the pressure of acetone) against the peak area (number of acetone molecules adsorbed to the surface) a good fit may be achieved (Figure 10B) with $z = 4$ and $\omega = 2.1$ kJ mol^{-1}. Taking $z = 4$ is appropriate for the cubic unit cell of UO_2, and the value of 2.1 kJ mol^{-1} is of the order of magnitude of

(65) Adamson, A. W.; Gast, A. P. *Physical Chemistry of Surfaces*; Wiley: New York, **1997**.

Scheme 2. Summary of the Species Identified from the Adsorption of Acetone on the UO_2 Surface with IR Frequencies for the C−O Bond

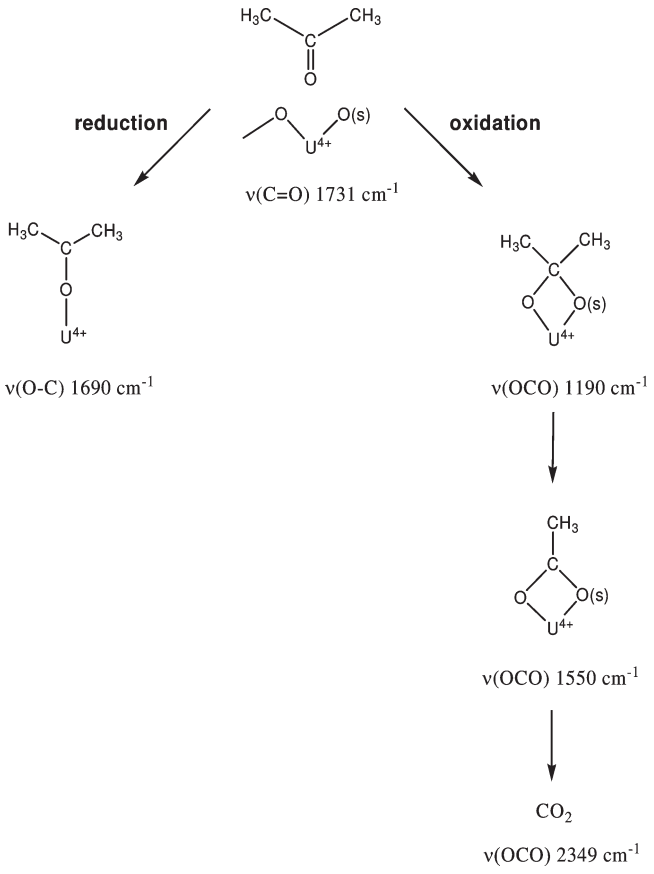

the van der Waals forces. Adamson and Gast[65] suggest that a typical value for β (equal to $z\omega/RT$) is 2.5 for a liquid that obeys Trouton's rule (enthalpy of vaporization = 85 J K^{-1} mol^{-1}). In this case, using the values derived above, β would equal 3.4, in keeping with the higher enthalpy change of vaporization for acetone. It can also be seen that the isotherm does not appear to saturate; after the injection of larger doses of acetone, the amount adsorbed continues to rise. The isotherm plotted in this case has an overall appearance of Brunauer's type V isotherm. This type of isotherm is often seen in multilayer adsorption onto porous materials. Initially, little adsorption occurs, but then islands form as a result of adsorbate−adsorbate interactions and finally the isotherm levels off as saturation occurs.

It is clear from the discussion that the adsorption process in this experiment cannot be represented by a simple model; both adsorbate−surface and adsorbate−adsorbate interactions are present. The adsorbate−adsorbate interactions may be direct such as those that occur between liquid molecules (i.e., van der Waals forces and hydrogen bonding) or indirect, mediated through electronic changes in the surface. It is not possible to distinguish between these two types of interaction experimentally by TPD. Multilayer formation has been noted in other adsorption studies involving acetone, notably by Henderson[44] on TiO_2(110) and by Anton et al.[48] on the clean, oxygen-activated Ru(001) surface. It is also noteworthy that both Anton et al.[48] and Liu and Vannice[66] suggest island formation prior to complete monolayer coverage during their studies on the Ru(001) and Pt foil.

3.B.4. Reaction Order. The reaction order may be determined by means of an Arrhenius plot.[67] In this method, a spectrum is plotted as $\ln(r/\theta^n)$ against $1/T$ for $n = 0$, 1, and 2. A linear relationship is found for the plot corresponding to the correct reaction order. Average values for the activation energy and the pre-exponential factor may be derived from the slope and the intercept, respectively. The results for the spectra recorded for m/z 15 (Figure 11) show that the reaction is close to second order. This fragment is derived from products formed by a range of reactions and thus would be unlikely to yield an integer-order relationship. The Arrhenius plot for m/z 58 yields a reaction order of one for the desorption reaction; this is expected because the adsorption of acetone was shown to be molecular by the infrared data.

3.B.5. Activation Energy. 3.B.5.a. Variation of Heating Rate. To calculate the activation energy of the system using standard redhead analysis,[68] the value of the pre-exponential factor must to be assumed. To avoid the need to make this assumption in this study, the heating rate was varied. Ideally, this should have been over two or more orders of magnitude; however, such a wide range was difficult to achieve experimentally, and heating rates between 0.1 and 0.4 K s^{-1} were used. Experiments were performed at saturation coverage.

The TPD spectra of m/z 15 at saturation coverage and at various heating rates are shown in Figure 12. The slowest heating rate, 0.1 K s^{-1}, produced a low, broad peak composed of at least two unresolved peaks; the faster heating rates caused these two peaks to coalesce, and a taller peak indicating a faster desorption rate was observed. The peak maximum was seen to shift to a higher temperature with higher heating rates. Taking the peak maximum for the first peak in each case and plotting $1/T_p$ against $\ln(\beta/kT_p^2)$, a value of 32 kJ mol^{-1} was calculated for the activation energy (inset). This method was applicable only to the lowest-temperature peak in each case. The activation energy calculated by this method is on the order of magnitude of hydrogen bonding interactions. Hydrogen bonding can occur between acetone molecules, and this may indicate that island formation is occurring prior to complete monolayer coverage, similar to that seen on Ru(001) surfaces.[48]

3.B 5.b. Leading-Edge Analysis. Habenschaden−Kuppers or leading edge analysis[69] was used to calculate a value for the activation energy and pre-exponential factor for both m/z 15 and 58. The data for mass fragment 58 are presented whereas those for corresponding mass fragment 15 are omitted for simplicity. The values for activation energies extracted are presented in Table 5 for both masses. For mass fragment 58, initial coverage values of 0.33, 0.76, and 1.0 monolayer corresponding to the injection of 5, 10, and 15 μL, respectively, were used. These activation energy values were obtained from the Arrhenius plot of ln(pressure), equal to the change in coverage, against $1/T$ for the first 4% change in coverage. As shown in the Table, there is some trend of decreasing E_d with increasing coverage, yet the scattering of the data and the unrealistic E_d for m/z 58 suggest that the method is not adequate.

(66) Liu, Z. M.; Vannice, M. A. *Surf. Sci.* **1994**, *316*, 337.
(67) Niemantsverdriet, J. W.; P. Dolle, P.; Markert, K.; Wandelt, K. *J. Vac. Sci. Technol., A* **1987**, *5*, 875.
(68) Redhead, P. A. *Vacuum* **1962**, *12*, 203.
(69) Habenschaden, E.; Kuppers, J. *Surf. Sci.* **1984**, *138*, L147.

Table 3. Fragmentation Patterns for Acetone and the Reaction Products Used in the Analysis of TPD Data[c]

	mass fragments																		
species	98	84	83	69	58	55	45	44	43	42	41	39	29	27	26	18	15	14	2
acetone[a]					1				10				9	9	10		100	43	
2,3-DMB[b]		31		81		16			8	9	100	33		19					
mesityl oxide[a]	3		10			22			95	18	13	70	40	64	16		100	23	
propene[b]										70	100	72		39	11				
isopropanol[a]							5	10					18	20	10	8	100	26	
CO_2[b]								100											
H_2O[b]																100			
H_2[b]																			100

[a] Data derived from the instrument. [b] Data derived from reference values.[19] [c] 2,3-DMB = 2,3-dimethylbutene.

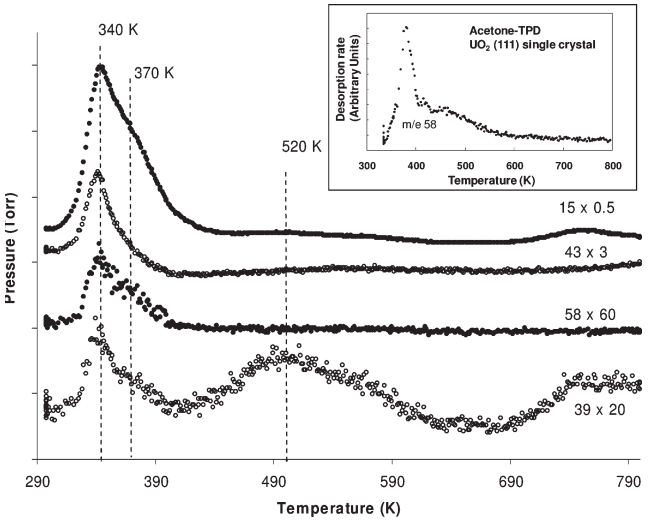

Figure 7. TPD spectra, from the reaction of acetone on polycrystalline UO_2, showing major mass fragments from unreacted acetone. The saturation coverage is 20 μL injection/1 g of UO_2 with a heating rate 0.25 K s^{-1}. (Inset) TPD after acetone adsorption at 300 K over UO_2(111) single crystals.

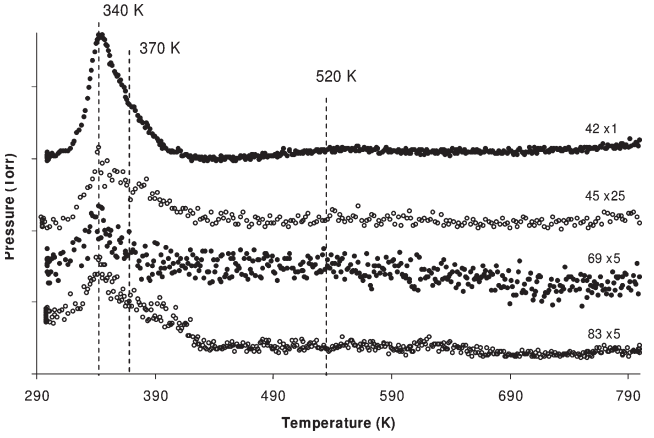

Figure 8. TPD trace for the unique mass fragments of the reaction products propene (m/z 42), isopropanol (m/z 45), 2,3-dimethylbutene (m/z 69), and mesityl oxide (m/z 83). TPD was performed at saturation coverage, with an injection of (20 μL/L g UO_2) acetone and a heating rate of 0.25 K s^{-1}.

3.B.5.c. Complete Analysis. Data from mass fragments 15 and 58 were also treated to a "complete analysis".[70,71] The coverage curves were plotted first as shown in Figure 13.

(70) King, D. A. *Surf. Sci.* **1975**, *47*, 384.
(71) Taylor, J. L.; Weinberg, W. H. *Surf. Sci.* **1978**, *78*, 259.

Table 4. TPD Data Analysis at Saturation Coverage and Heating Rate 0.25 K s^{-1}, Showing the Products with Their Identifying Mass Fragments, Temperature of Evolution, and Percent Relative Abundance

	m/z	temperature (K)	relative abundance (%)
acetone	58	340, 370	45
propene	42	340, 370, 520	44
mesityl oxide	83	340, 370	6
isopropanol	45	340, 370, 520	2
2,3-dimethlybutene	69	370	2
CO_2	44	600+	0.5

From these curves, the ln(desorption rate) and $^1/_T$ for fixed coverage values were determined, and Arrhenius plots were prepared. The corresponding activation energies and pre-exponential factors derived from the slope and intercept, respectively, are given in Table 6. The activation energies and prefactors present some trend, with realistic numbers indicating that the method might be suitable for acetone desorption. It is to be noted that unreacted acetone represents about 50% of the surface coverage because the other half reacts to give other products. It was not possible to determine a trend in the coverage dependence of the activation energy in the case of m/z 15. This might be partially explained by the presence of more than one peak and hence more than one adsorption site; the effect of coverage on the value of the activation energy of each peak may be different, effectively canceling each other. This is supported by the Arrhenius plot (n = 2) and the finding that the activation energy did not change significantly with coverage, yet there was an observed shift in the peak maximum. However, the pre-exponential factor does show a trend—decreasing with increasing coverage. The activation energy and pre-exponential factor for m/z 58 show a more definite trend—both are decreasing with increasing coverage. This finding, together with the shift in peak position, is in line with the Arrhenius plot (n = 1), suggesting that the desorption reaction is first order, which supports the IR result that indicated molecular adsorption.

Activation energies for acetone on other metal and metal oxide surfaces have mostly been calculated by simple redhead analysis, assuming a value for the pre-exponential factors of $10^{13}-10^{14}$ s^{-1}. Henderson[44] acknowledges the inadequacy of the redhead analysis in his study on TiO_2(110) and suggests that there is likely to be a coverage dependence of the activation energy due to the shift to lower temperature of the leading edge and the peak of the TPD trace. He postulated that there are likely to be repulsive acetone−acetone interactions and goes on to suggest that the onset of these acetone−acetone repulsions is likely to be

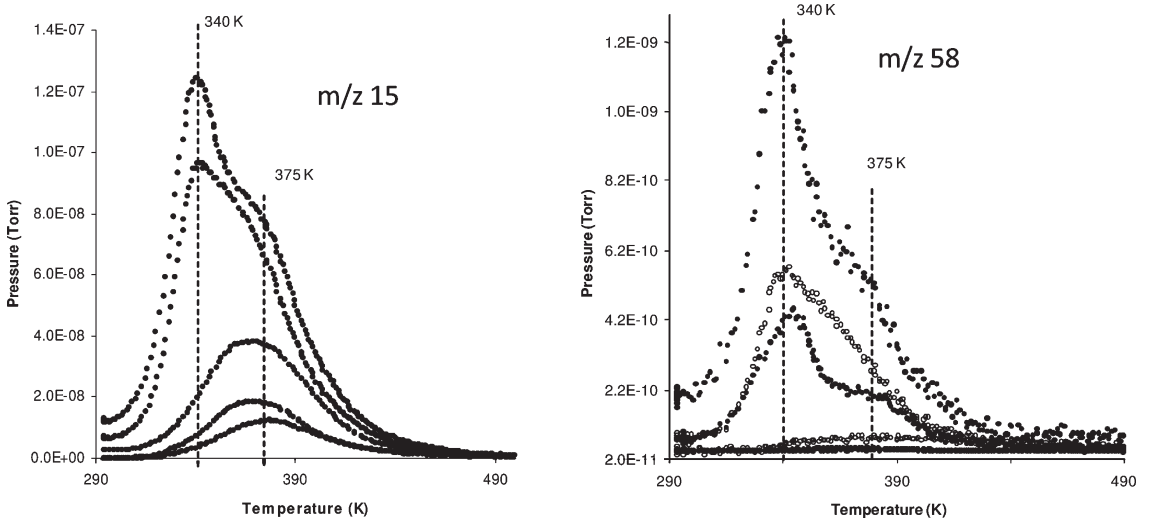

Figure 9. TPD traces for m/z 15 and 58 showing the effect of increasing coverage, where successive lines correspond to the injection of 3, 5, 10, 15, and 30 μL of acetone for the temperature region of 290 to 500 K. Heating rate 0.25 K s^{-1}. Catalyst weight 1 g.

Scheme 3

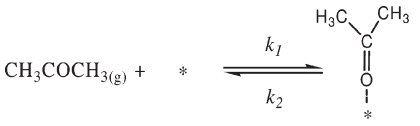

at about 0.5 ML coverage when adjacent Ti^{4+} sites must be occupied. A value of 97−105 kJ mol^{-1}, assuming 10^{14} s^{-1} for the prefactor, is given for the adsorption of d_6-acetone onto the TiO_2(110) surface.[44] Houtman et al.[51] calculated a figure of 70 kJ mol^{-1}, assuming a pre-exponential factor of 10^{13} s^{-1}, for the adsorption of acetone on Rh(111)−(2 × 2)O. Anton et al [48] gives a range of 42−63 kJ mol^{-1} for a clean Ru (001) surface and 42−79 kJ mol^{-1} for the Ru(001)−p(2 × 2) O surface. Finally, Avery[50] quotes 48 kJ mol^{-1} for adsorption onto the Pt(111) surface.

The different methods used in the analysis of the data to determine the activation energy and the pre-exponential factor have given results that can largely be grouped into those at low initial coverage derived from the complete analysis and those at high coverage derived from the leading edge analysis. It could be construed that the trend seen in the activation energy and the pre-exponential factor for m/z 58 is a product of the method used and not a true trend. It is difficult to counter this argument emphatically with the data available; however, de Jong et al.[72] have published work comparing the 10 most commonly applied methods of analysis. In this paper, the authors suggest that there is generally good agreement between the methods applied here, namely, the complete analysis and the Habenschaden−Kuppers or leading edge analysis. Results derived from the variation in heating rate were also reported to be close to the true values and within acceptable error. A determination of the reaction order from the fit of the data to the Arrhenius plot was considered to be an acceptable method; however, a determination of the activation energy and pre-exponential factor from this plot was not recommended. Simple methods such as the Redhead analysis were also found to perform poorly and should not be relied upon. Seebauer[73] has noted that in systems that show molecular adsorption the prefactor

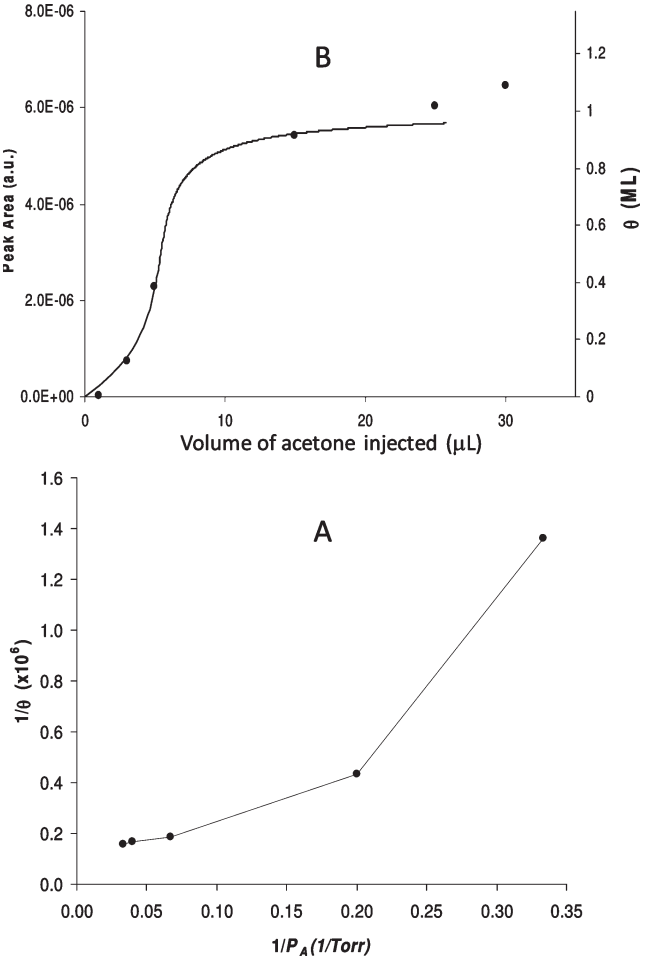

Figure 10. (A) Langmuir isotherm plot of $1/\theta$ against $1/P_A$ for the experimental coverage curves (mass 15) showing the nonlinear relationship. (B) Modified Langmuir isotherm to account for lateral interactions. Data are shown for m/z 15. $z = 4$, and $\omega = 2.1$ kJ mol^{-1}.

commonly takes values greater than 10^{13} s^{-1} and that in many systems decreases in the prefactor of 10^6 with increasing coverage are observed. Nieskens[74] states that in adsorption

(72) de Jong, A. M.; Niemantsverdriet, J. W. *Surf. Sci.* **1990**, *233*, 355.
(73) Seebauer, E. G. *Surf. Sci.* **1994**, *316*, 391.
(74) Nieskens, D. L. S.; van Bavel, A. P.; Niemantsverdriet, J. W. *Surf. Sci.* **2003**, *546*, 159.

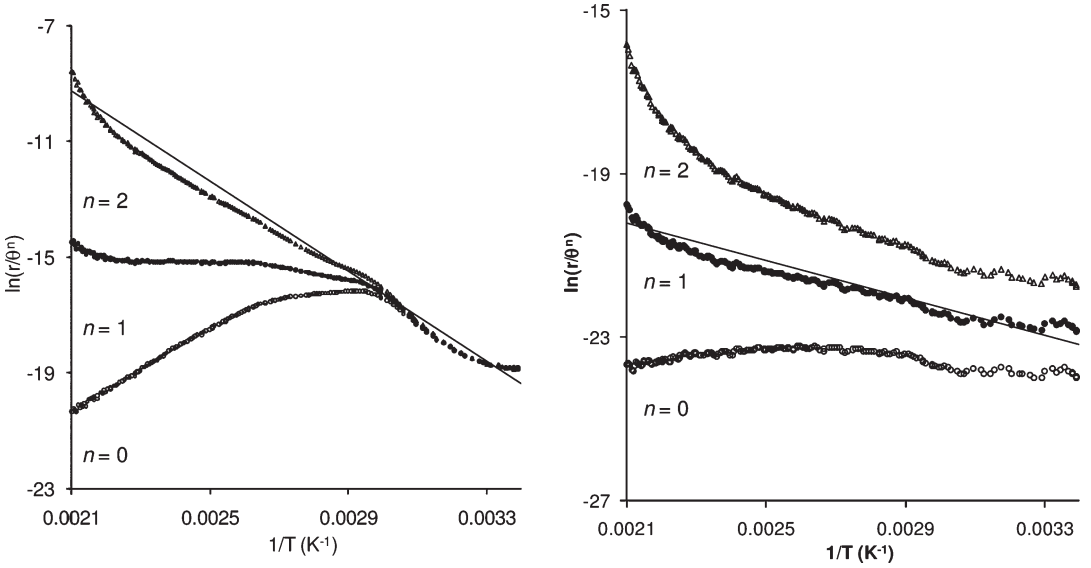

Figure 11. Arrhenius plot for (A) m/z 15 and (B) m/z 58, extracted from acetone TPD.

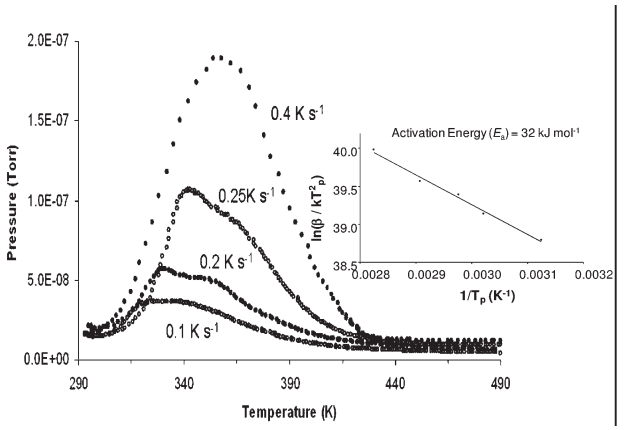

Figure 12. TPD spectra for m/z 15 and acetone on UO_2 at saturation coverage. The plot shows the effect of the variation in heating rate. (Inset) Plot of $1/T_p$ against $\ln(\beta/kT_p^2)$.

systems in which lateral interactions are present the kinetic parameters often show a dependence on coverage.

A relationship between the activation energy and the prefactor is commonly seen, and if it is linear, it constitutes the compensation effect.[71,75] This relationship, also termed the Cremer−Constable relation, is given by the equation

$$E_a(\theta) = \alpha_1 \ln \nu_d(\theta) + \alpha_2 \quad (9)$$

where α_1 and α_2 are constants. In delineating such compensation effects, care must be taken in that they are not induced through the treatment of the data. An example of such a false compensation effect is given by Miller[76] and results from the practice of using the slope of an Arrhenius plot to derive a value for the activation energy. The slope of such a plot is given by the expression

$$\text{slope} = \frac{\partial \ln\left(\frac{r}{\theta^n}\right)}{\partial\left(\frac{1}{T}\right)} = \left[\frac{-E_a}{R}\right]_\theta + \frac{\partial\theta}{\partial\left(\frac{1}{T}\right)}\left[\frac{\partial \ln \nu_d(\theta)}{\partial(\theta)} - \frac{1}{RT}\left(\frac{\partial E_a(\theta)}{\partial\theta}\right)\right]_T \quad (10)$$

The second term in the equation is commonly ignored, and by putting a straight line through the points, a compensation effect is forced on the data. This approach can be used only when the coverage is constant and $\partial\theta/\partial(1/T)$ equals zero, as in the case of the complete analysis and to a good approximation in the leading edge analysis. Although the coverage is kept constant in the complete analysis, care still needs to be exercised in the interpretation of the results. Nieskens et al.[74] have shown that for an accurate determination of the coverage small temperature steps on the order of 0.2 to 0.5 K are required. When the step size is increased to between 0.75 and 1.0 K, as used in this study, then the change in coverage, even though small (0.005 ML), is sufficient to cause scatter in the data and may lead to the development of false trends.

An explanation for the compensation effect from first principles has not yet been determined, but many ideas based on transition-state theory have been put forward. One such is given by Taylor and Weinberg,[71]71 in which the natural logarithm of the pre-exponential factor is proportional to the entropy difference between the activated and adsorbed phases

$$\ln \nu_d = \frac{S* - S^s}{k} \quad (11)$$

where S^* is the entropy of the activated complex and S^S is the entropy of the adsorbed phase. The change in the prefactor is caused by an increase in the entropy of adsorption with coverage or a decrease in the entropy of the activated complex with coverage. Either of these conditions is plausible; an adsorbate that binds less strongly with increasing coverage, reducing the effective barrier to surface diffusion and hence becoming more mobile, will show an increase in the entropy of adsorption, the first condition. The entropy of the activated complex may decrease with increasing coverage because the population of the activated species increases and entropy decreases with increasing population.

(75) Bond, G. C.; Keane, M. A.; Kral, H.; Lercher, J. A. *Catal. Rev. Sci. Eng.* **2000**, *42*, 323.
(76) Miller, J. B.; Siddiqui, H. R.; Gates, S. M.; Russell, J. J. N.; Yates, J. J. T.; Tully, J. C.; Cardillo, M. J. *J. Chem. Phys.* **1987**, *87*, 6725.

Table 5. Activation Energy and Pre-exponential Factor Calculated by Leading Edge Analysis for *m*/*z* 15 and 58 for the First 4% Reduction in Coverage

volume of acetone injected (μL)	initial coverage θ_0 (ML)	activation energy (kJ mol^{-1})
	m/*z* 15	
3	0.16	88
5	0.46	32
15	1.0	40
25	1.2	29
	m/*z* 58	
5	0.33	19
10	0.76	25
15	1.00	12

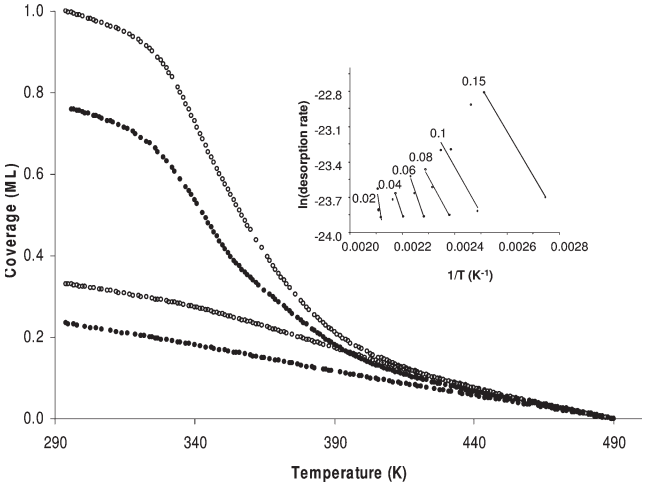

Figure 13. Coverage curves for *m*/*z* 58 and acetone on UO_2. Curves for initial coverage values of 1.0, 0.76, 0.33, and 0.23 corresponding to the injection of 15, 10, 5, and 3 μL of acetone are shown. (Inset) Arrhenius plot for the complete analysis of *m*/*z* 58.

4. Conclusions

The reactions of acetone have been studied by FTIR and TPD over polycrystalline UO_2. IR data indicate that acetone is adsorbed molecularly in the η^1(O) mode. A σ bond is formed from the donation of the lone pair on the carbonyl oxygen to a Lewis acid site (uranium cation) on the UO_2 surface. In addition, isopropoxides were present on the surface and formed as intermediates in the deoxygenation reaction producing propene and isopropanol, with both products seen in the TPD experiments. On heating, acetone and isopropanol desorb at about 500 K. Further heating results in the formation of surface acetates, which subsequently decompose to carbon dioxide. TPD on polycrystalline UO_2 indicated that the major product of the interaction is unreacted acetone, a finding in keeping with the IR data that showed molecular adsorption. Of the reactions that do take place, the deoxygenation reaction was the most productive. Other significant reactions that occurred included reductive coupling and aldol condensation. UO_2 has similar activity to nearly stoichiometric TiO_2 in this respect. The adsorption of acetone does not fit the simple Langmuir model, and adsorbate−adsorbate interactions are significant. The desorption of acetone from the surface is a first-order reaction, with a coverage-dependent activation energy and pre-exponential factor. The complete analysis method of TPD data gave the most realistic activation energy, E_d, and prefactor, with E_d changing from 135 kJ/mol at nearly zero coverage to about 35 kJ/mol at $\theta = 0.15$.

Table 6. Activation Energy and Pre-Exponential Factor from the Complete Analysis of *m*/*z* 15 and 58

coverage	activation energy (kJmol^{-1})	k_0 (s^{-1})
	m/*z* 15	
0.02	42	10^7
0.03	27	10^{11}
0.05	26	10^{11}
0.06	28	10^{10}
0.07	28	10^9
0.18	24	10^9
0.20	30	10^7
0.25	37	10^5
0.30	40	10^4
	m/*z* 58	
0.02	137	10^{13}
0.04	58	10^{14}
0.06	54	10^{14}
0.08	33	10^9
0.10	33	10^{14}
0.15	32	10^{11}